

**The Heat Treatment Severity Index: A new metric correlated to the properties of biochars obtained from entrained flow pyrolysis of biomass**

Chamseddine Guizani, Mejdj Jeguirim, Sylvie Valin, Marine Peyrot, Sylvain Salvador

► **To cite this version:**

Chamseddine Guizani, Mejdj Jeguirim, Sylvie Valin, Marine Peyrot, Sylvain Salvador. The Heat Treatment Severity Index: A new metric correlated to the properties of biochars obtained from entrained flow pyrolysis of biomass. Fuel, Elsevier, 2019, 244, pp.61-68. 10.1016/j.fuel.2019.01.170 . hal-02011636

**HAL Id: hal-02011636**

**<https://hal-mines-albi.archives-ouvertes.fr/hal-02011636>**

Submitted on 12 Feb 2019

**HAL** is a multi-disciplinary open access archive for the deposit and dissemination of scientific research documents, whether they are published or not. The documents may come from teaching and research institutions in France or abroad, or from public or private research centers.

L'archive ouverte pluridisciplinaire **HAL**, est destinée au dépôt et à la diffusion de documents scientifiques de niveau recherche, publiés ou non, émanant des établissements d'enseignement et de recherche français ou étrangers, des laboratoires publics ou privés.

# The Heat Treatment Severity Index: A new metric correlated to the properties of biochars obtained from entrained flow pyrolysis of biomass

Chamseddine Guizani<sup>a,\*</sup>, Mejdı Jeguirim<sup>b</sup>, Sylvie Valin<sup>c</sup>, Marine Peyrot<sup>c</sup>, Sylvain Salvador<sup>d</sup>

<sup>a</sup> Aalto University, School of Chemical Engineering, Department of Bioproducts and Biosystems, Vuorimiehentie 1, 02150 Espoo, Finland

<sup>b</sup> Institut de Sciences des Matériaux de Mulhouse, 15 rue Jean Starcky, 68057 Mulhouse, France

<sup>c</sup> CEA, LITEN/DTBH/SBRT/LTB, 38054 Grenoble cedex 09, France

<sup>d</sup> RAPSODEE, Mines Albi, CNRS UMR 5302, Route de Teillet, 81013 ALBI CT Cedex 09, France

## A B S T R A C T

The properties of biochars produced in biomass pyrolysis processes highly depend on the pyrolysis conditions, specifically the pyrolysis temperature and thermal treatment duration. The higher the temperature and the duration, the more severe is the heat treatment. The present work proposes a new Heat Treatment Severity Index (HTSI) for the quantification of the heat treatment severity during the pyrolysis reaction. This metric takes into account both effects of reactor temperature and heat treatment time inside the reactor. The relevance of this HTSI is assessed through analyzing the evolution of some properties of biochars obtained after pyrolysis of 370  $\mu\text{m}$  beech wood particles in an entrained flow reactor. These biochars were characterized for their chemical composition (elemental analysis), structure (Raman spectroscopy) and reactivity towards oxygen (thermo-gravimetric analysis). These properties were well correlated with the HTSI following remarkable mathematical relationships. This finding demonstrates the possibility to engineer biochars with controlled properties by a careful mastering of the experimental conditions of the pyrolysis process in terms of temperature and heat treatment time.

### Keywords:

Biomass

Entrained flow pyrolysis

Biochar properties

Heat Treatment Severity Index

## 1. Introduction

Currently, biomass is a crucial energy source allowing the shift from a fossil fuels based economy to bio-resources based one. Various thermochemical processes are available for the biomass conversion to energy or to alternative fuels [1]. Among these processes, pyrolysis is an attractive technique allowing the transformation of the raw biomass into biofuels with a higher energy density including bio-oil and biochar [2].

Hans-Peter Schmidt listed no less than 55 potential uses of biochar [3]. These include for instance gasification for syngas production, adsorption for gas or liquid purification, catalysis in diverse reactions as well as the use in soil fertilization [4,5]. The selection of the suitable valorization strategy depends strongly on the biochar characteristics such as chemical composition, surface functional groups and textural properties [6,7]. These characteristics are influenced by the pyrolysis conditions such as the reactor temperature, the particle size and heating rate as well as the residence time [8,9].

Among these characteristics, the biochar chemical composition is strongly affected by the pyrolysis temperature. Uchimiya et al. have

compared the elemental composition of chars prepared from the slow pyrolysis of cottonseed hull at five temperatures (200, 350, 500, 650, and 800 °C). Authors have observed that O and H atoms are released in the gas phase when temperature increases. In particular, the O/C molar ratio decreased from 0.59 to 0.06 and the H/C molar ratio decreased from 1.38 to 0.08 when temperature increased from 200 to 800 °C [10]. This O and H release is due to the thermal degradation of biomass components namely, cellulose, hemicellulose and lignin as well as the residual biochar cracking. In contrast, no significant effect of temperature was observed on N content in the residual biochar.

The effect of the heating rate on the biomass biochar composition was also examined in literature. Although heating rate has a significant effect on the biochar yield, no clear difference was observed for biochar compositions when they were prepared at various heating rates for similar pyrolysis temperature. Onay and Kockar observed a similar chars composition during the slow, fast and flash pyrolysis of rapeseed at 550 °C [11].

The surface functionality of biomass biochar is also affected by the pyrolysis operating conditions. In particular, biochar oxygen functionality is progressively eliminated with increasing pyrolysis temperature

\* Corresponding author.

E-mail address: [chamseddine.guizani@aalto.fi](mailto:chamseddine.guizani@aalto.fi) (C. Guizani).

[12]. Hence, carboxylic groups are decomposed to CO<sub>2</sub> at 100–400 °C while the removal of lactones and carboxylic anhydrides occurs at 427–657 °C. The highest thermally stable C-O groups are pyrone (900–1200 °C) followed by ethers, carbonylic and quinonic groups, and phenolic and hydroquinic groups [13]. The removal of surface oxygen groups when pyrolysis temperature increases is attributed to different reactions including dehydration, decarboxylation and decarbonylation. These reactions lead to the condensation and the growth of small aromatic structures [14].

The structural properties also change with pyrolysis temperature and biochar residence time. The local order in the biochar structure increases when increasing the temperature and heat treatment time. However, in chars this order is typically confined to the growth of graphene-like domains a few nanometers across with the structure remaining mainly porous and disordered at larger distances. The biochar pores are also between hexagonal layers. The ordering of the structure helps create pores through a rearrangement of the amorphous carbon structures into denser graphene-like domains with increasingly severe heat treatments [15,16]. Zhao et al. have analyzed biochar structural properties using Raman spectroscopy for different feedstock sources and pyrolysis temperature [17]. They observed that both Raman D and G bands were present in chars after a pyrolysis temperature of 500 °C.

These biochars had an I<sub>D</sub>/I<sub>G</sub> ratio ranging between 0.804 and 1.51. The authors mentioned that the ratio of strongly distorted or disordered structures of turbostratic carbon to ordered graphite crystals was strongly influenced by pyrolysis temperature. Furthermore, the heating rate has a significant effect on biochar structural properties. Brewer et al. have compared biochars' characteristics during slow and fast pyrolysis as well as gasification process [16]. They noted a marked decrease in aromatic C-H functionality between slow pyrolysis and gasification chars using Nuclear Magnetic Resonance and Infrared spectroscopy spectra. In addition, NMR estimates of fused aromatic ring cluster size presented a similar structure from fast and slow pyrolysis (7–8 rings per cluster), while biochar was much more condensed (17 rings per cluster) at higher temperature gasification [18].

The biochar textural properties (pore size distribution, surface area, pore volume...) are influenced by the pyrolysis conditions and also strongly by the feedstock sources [19]. The available results in literature showed a large variability in micropores volume and surface area values. In general, low values for textural parameters are obtained below 450 °C and the highest values of micropores volumes and surface areas are typically obtained at 500 °C–900 °C [10]. A low surface area comes from lack of atomic size pores within hexagonal carbon layers and pore blockage by condensed volatile matters.

The biochar pores are also between hexagonal layers. The ordering of the structure could help create pores through a rearrangement of the amorphous carbon structures into denser graphene-like domains with increasingly severe heat treatments.

It is also worth mentioning that CO<sub>2</sub> adsorption manometry may be more appropriate than the commonly used N<sub>2</sub> adsorption manometry for detecting the microporosity of biochars, since CO<sub>2</sub> accesses more easily to these small pores (< 1 nm) than N<sub>2</sub> [18].

The determination of the biochar characteristics, detailed previously, requires expensive analytical techniques and highly trained and competent scientists or engineers. Therefore, the identification of correlation between biochar properties and other parameters related to the experimental conditions would be of real interest for the assessment of chars' suitability for various applications, potential rapid industrial quality control procedures in the future, and for understanding more fundamental aspects of the fine structural changes which occur during the pyrolysis and subsequent heat treatment process. Several attempts have been performed to identify correlations between pyrolysis conditions, biochars properties and reactivity measurements. McDonald-Wharry et al. [20] showed that the I<sub>V</sub>/I<sub>G</sub> Raman structural ratio was correlated with heat treatment temperature for various types of chars. Morin et al. observed a decrease of beech biochar reactivity with an

increasing pyrolysis temperature [21]. Several authors also correlated biochar properties such as structural parameters, specific surface area and pore volume of the biochar and their combustion and gasification reactivities [22–25].

In previous related works, we studied the evolution of chars properties obtained after pyrolysis of 370 μm beech wood particles in an entrained flow reactor in a temperature range between 500 °C and 1400 °C [26,27]. These chars were characterized for their chemical composition (Elemental analysis), structure (Raman spectroscopy) and reactivity towards oxygen (thermogravimetric analysis) [28]. The yield, chemical composition, surface chemistry, structure, morphology and reactivity of the chars were highly affected by the pyrolysis temperature. In addition, some of these properties related to the biochar structure and chemical composition were found to be correlated to the biochar reactivity. Also, we have found that the structure and chemical composition of these chars were well correlated through a remarkable relationship between the (O + H)/C atomic ratio and I<sub>V</sub>/I<sub>D</sub> structural parameter [29].

Our previous works as well as the literature overview well demonstrate that the biochar properties are dependent on the pyrolysis conditions in terms of reactor temperature and heat treatment time, which can be viewed as indicators of the Heat Treatment Severity.

The definition of a severity factor or index for various type of biomass pretreatment and treatment reactions, such as for the steam explosion, pre-hydrolysis or acid hydrolysis, has been attempted and successfully set as a parameter for the description of the reaction severity [30]. A severity factor summarizing the effect of temperature and time during the hydrothermal carbonization of biomass allowed also finding clear tendencies in the production of hydrochars and derived carbons in terms of yield, composition, and surface area [31]. Other authors introduced an Integral Metric of Charring Intensity (CI) that combines the temperature and duration of pyrolysis to characterize the continuum of chemical transformations of biomass during the carbonization process [32]. The authors found two types of responses to CI: either linear or threshold relationships. Mass yield decreased linearly with CI, while a threshold existed across which %C, %N, and δ<sup>15</sup>N exhibit large changes.

We propose in this work a new definition for a severity index that correlates well with many of the biochar properties obtained from biomass entrained flow fast pyrolysis.

The biochars were prepared by an entrained flow pyrolysis of 370 μm beech wood particles between 500 °C and 1400 °C [26,27], and characterized for their chemical composition, structure and reactivity [28]. Leaning on the modeling results validated with the pyrolysis experiments in [26,27], which provide data on the biomass particle pyrolysis and residence times, and on the biochar properties described in our previous work [28], we searched for a suitable expression of a severity index that could be related directly on the measured biochar properties. This work is a first attempt for the investigation of this idea.

## 2. Material and methods

### 2.1. Raw biomass

Raw biomass used in this work is beech wood supplied by the Sowood company (France). The raw wood is finely ground with particles having sizes ranging from tens of microns to a few millimeters. After sieving, particles having a mean size of 370 μm were selected for the pyrolysis experiments. This mean size should be appropriate to avoid heat and mass transfer limitations during the EFR pyrolysis experiments.

The moisture content was determined by drying at 105 °C according to the NF-EN-14,774 standard. Ash content was determined by burning the sample in air at 850 °C according to the NF-EN-14775 standard. The oxygen content was determined by difference to the sum of C, H, N and ash contents. The proximate and ultimate analyses are shown in

**Table 1**  
Proximate and ultimate analyses of beech wood.

Proximate analysis	Moisture [wt% ar <sup>*</sup> ]	8.7
	Volatile Matter [wt% db <sup>**</sup> ]	84.3
	Fixed carbon [wt% db]	15.2
	Ash (815 °C) [wt% db]	0.5
Ultimate analysis [wt% db]	C	49.1
	H	5.7
	N	0.15
	S	0.045
	O (by difference)	44.5

\* ar: as received.

\*\* db: dry basis.

**Table 1.**

## 2.2. Experimental Entrained Flow Reactor (EFR) set up

The EFR experimental set-up was previously described in details in [26,27]. It consists of an alumina tube inserted in a vertical electrical heater with three independent heating zones. The dimensions of the tube are 2.3 m in length and 0.075 m in internal diameter. The heated zone is 1.2 m long. The EFR works at atmospheric pressure and can reach a maximum temperature of 1400 °C. The wood particles are continuously fed into the reactor using a gravimetric feeding system. The main N<sub>2</sub> gas stream is electrically pre-heated before entering the reactor. A sampling probe allows collecting the remaining solid in a settling box.

## 2.3. Pyrolysis conditions

The pyrolysis experimental conditions are as follows:

The biomass mass flow rate is set to a fixed value of 1 g/min. The mean particle size is 370 μm for all experiments. The gas residence time was controlled with the nitrogen flow rate, as the pyrolysis gas flowrate was much lower than the N<sub>2</sub> one. The mean gas residence time was determined knowing the nitrogen flowrate, the reactor temperature, length and cross-section.

The chars are produced from the biomass pyrolysis and gathered from two experimental campaigns with two different objectives:

- The first one is related to medium temperature pyrolysis (500, 550 and 600 °C) aiming at maximizing the bio-oil production [26].
- The second one concerns high temperature pyrolysis (800, 1000, 1200 and 1400 °C) aiming at maximizing the gas fraction [27].

To sum up, seven chars were thus obtained and well characterized as described in [28].

## 2.4. The GASPARG model

During the entrained flow pyrolysis, a biomass particle entering the top of the reactor of a length  $L$ , at the time  $t = 0$ , corresponding to the spatial coordinate  $Z = 0$  is heated by convection and radiation. It dries and gets pyrolyzed as its temperature increases. If the temperature is high enough, the pyrolysis process finishes at the time  $t_{pyr}$  at a position  $Z < L$  before it leaves the reactor. The biochar keeps going down in the reactor until it leaves at  $t_{res}$ , corresponding to the spatial coordinate  $Z = L$ . Between  $t_{pyr}$  and  $t_{res}$ , the biochar remains at a high temperature and is further heat-treated. A schematic illustration of these stages is shown in Fig. 1.

The GASPARG model [27,26,33,34] was developed to describe the pyrolysis and gasification of biomass particles in an EFR. It is a 1-D model that accounts for the main physical phenomena and chemistry related to the heterogeneous and gas phase reactions. The robustness and accuracy of the model for prediction of product yields was

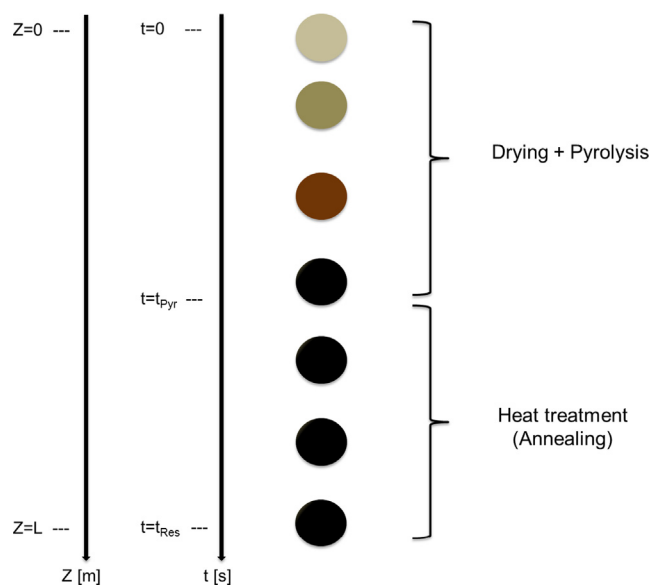


**Fig. 1.** Schematic representation of a biomass particle during entrained flow pyrolysis.

validated over a wide range of temperature, atmospheres and particle size [27,35].

In the present study, the GASPARG model was used for the calculation of (Fig. 1):

- the particle residence time  $t_{res}$  which is the residence time of the solid particle, regardless of its state (fresh biomass, pyrolyzing biomass or biochar) in the heated part of the reactor,
- the particle pyrolysis time,  $t_{pyr}$ , which is defined as the time at which the mass of solid particle is at less than 1% from its final value after complete devolatilization.

The entrained flow reactor is modeled as a plug flow reactor. Temperature and concentrations are supposed to be uniform inside the particles. Heat conduction inside the particles – 370 μm in the present study - is supposed to be much more rapid than pyrolysis chemical reaction. A characteristic time analysis based on the same principles as those described in [36], shows that this assumption is only valid for temperatures of 600 °C and below. For temperature higher than 800 °C, external heat transfer controls the pyrolysis rate, and the uniform particle temperature assumption does not have any significant influence on the results.

The particle residence time is calculated considering the slip velocity between solid particles and gas. The slip velocity depends on the particle density and size, and on their evolution as pyrolysis proceeds, between the density and size of wood particles and those of biochar particles [37].

Particle pyrolysis is modelled by a one-step reaction in which biomass is decomposed into gas species, tar and biochar. The kinetic of pyrolysis reaction follows an Arrhenius law in which the activation energy and pre-exponential factor are equal to 89500 J.mol<sup>-1</sup> and 1.483 × 10<sup>6</sup> s<sup>-1</sup> respectively [38].

## 2.5. Characterization techniques of the biomass chars

The characterization techniques of the chars comprising elemental analysis, Raman spectroscopy, SEM-EDX, FTIR spectroscopy as well as thermo-gravimetric analysis are described in [28]. The biochar chemical composition, structure through Raman spectroscopy and reactivity tests in air through thermo-gravimetric analysis were discussed in [28].

### 3. Results and discussion

#### 3.1. The Heat Treatment Severity Index (HTSI) definition

As discussed in the introduction part, as the biochar yield and properties are both temperature and heat-treatment time dependent, a severity index should account for both of those parameters to be relevant for the reaction severity description. We hypothesized that the HTSI should be the product of two terms:

- The first term would be obviously related to the heat treatment temperature of the biochar, which we defined as:

$$e^{\left(\frac{T_{\text{Reactor}}}{T_{\text{Ref}}}\right)}$$

$T_{\text{Ref}}$  and  $T_{\text{Reactor}}$  are respectively a reference temperature and the reactor temperature expressed in Kelvin. The value of the reference temperature can be arbitrary fixed. Strong correlations between the different biochar properties and the HTSI can be obtained for any arbitrary  $T_{\text{Ref}}$  value chosen as a constant between 400 and 600 K ( $R^2 = 0.96\text{--}0.99$ ). Regarding those results, we chose to fix  $T_{\text{Ref}}$  so as to maximize the average  $R^2$  calculated from the different correlations.

- The second term is related to the biochar heat treatment duration and defined as:

$$\left(\frac{t_{\text{Res}}}{t_{\text{Pyr}}}\right)$$

where  $t_{\text{Res}}$  and  $t_{\text{Pyr}}$  defined previously are expressed in seconds.

Three particular situations can be distinguished:

- o  $\left(\frac{t_{\text{Res}}}{t_{\text{Pyr}}}\right) < 1$ : the biomass particle is not completely pyrolysed
- o  $\left(\frac{t_{\text{Res}}}{t_{\text{Pyr}}}\right) = 1$ : the biomass particle is completely pyrolysed but the biochar leaves the reactor without any extra heat treatment
- o  $\left(\frac{t_{\text{Res}}}{t_{\text{Pyr}}}\right) > 1$ : the biomass particle completely pyrolysed and the biochar is heat treated in the reactor.

The expression for the Heat Treatment Severity Index reads:

$$HTSI = \left(\frac{t_{\text{Res}}}{t_{\text{Pyr}}}\right) e^{\left(\frac{T_{\text{Reactor}}}{T_{\text{Ref}}}\right)} \quad (1)$$

The values of  $t_{\text{Res}}$  and  $t_{\text{Pyr}}$  obtained from the simulation results, as well as the calculated HTSI for the different pyrolysis experiments are given in Table 2.

Only the 500 °C condition results in a non-completely formed biochar. However, as the pyrolysis conversion was high for this condition (94% based on subsequent mass loss upon heating at 500 °C in a thermo-gravimetric analyzer), we judged interesting to include it in our analysis. The different biochars are labeled as: Biochar - HTSI - (HTSI number) as shown in Table 2.

**Table 2**

Pyrolysis experimental conditions in the EFR and derived particle residence time and pyrolysis time from the modeling results.

Reactor temperature $T_{\text{Pyr}}$ [°C]	Gas residence time [s]	Particle residence time $t_{\text{Res}}$ [s]	Particle pyrolysis time $t_{\text{Pyr}}$ [s]	Heat Treatment Severity Index $HTSI$ [-]	Biochar label
500	16.6	2.99	5.75	2.00	Biochar-HTSI-1
550	16.6	4.57	2.64	7.28	Biochar-HTSI-2
600	16.6	5.68	1.37	19.02	Biochar-HTSI-3
800	4.9	2.27	0.35	42.18	Biochar-HTSI-4
1000	4.9	2.38	0.19	116.09	Biochar-HTSI-5
1200	4.9	2.51	0.098	334.73	Biochar-HTSI-6
1400	4.9	2.48	0.091	504.35	Biochar-HTSI-7

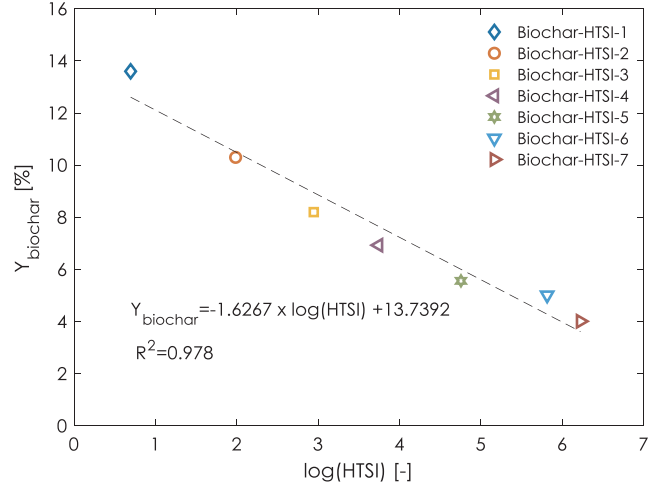


**Fig. 2.** Char yield as a function of log (HTSI).

#### 3.2. Biochar yield

The biochar yield was determined by weighing of the solid recovered in the biochar collection pot for the 500–600 °C experiments. For all the other experiments performed above 800 °C, about 80% of the products were sampled. The biochar yield was then calculated using the ash tracer method, as described in [25]. The biochar yield decreased from 14% at 500 °C to 4% at 1400 °C corresponding respectively to HTSI values of 2.00 and 504.35. The decrease of biochar yield with higher HTSI is likely due to faster heating rates at higher temperatures, shorter volatiles residence time in the biomass particle and promotion of volatiles/char cracking reactions into light gases instead of their cross-linking into a solid secondary char [39,40].

The biochar yield as a function of the HTSI is shown in Fig. 2. We found that the biochar yield is linearly correlated to the natural logarithm of HTSI ( $R^2 > 0.97$ ) following the relation:

$$Y_{\text{biochar}} = -1.6267 \log(HTSI) + 13.7392 \quad (2)$$

Although the correlation is good, this equation might only be appropriate to our fast-pyrolysis setup, feedstock and conditions. Further investigations will be needed to determine if a version of HTSI can be used to predict yield in other pyrolysis/carbonization systems and with other feedstocks.

Precaution is necessary here because several experimental parameters such as the particle size, gas flow rate, or heating rate can modify the biochar yield. For instance, in slow pyrolysis conditions, biochar yield change is quite low once the biochar has reached high enough temperatures (minor mass loss between 700 and 1400 °C in an oxygen free environment). Moreover, a multistep pyrolysis heating procedure can induce an increase of the biochar yield even after a subsequent higher temperature treatment step [41].

**Table 3**  
Chemical composition and atomic ratios for the different chars.

Sample	C [mol % afb]	H [mol % afb]	O [mol % afb]
Biochar-HTSI-1	47.1 ± 2.3	37.5 ± 0.8	15.4 ± 1.5
Biochar-HTSI-2	56.1 ± 1.3	32.4 ± 0.8	11.6 ± 0.5
Biochar-HTSI-3	63.4 ± 2.7	26.8 ± 1.1	9.9 ± 1.5
Biochar-HTSI-4	64.2 ± 1.5	26.9 ± 0.9	8.9 ± 0.6
Biochar-HTSI-5	74.4 ± 3.1	15.0 ± 0.2	10.6 ± 2.8
Biochar-HTSI-6	77.6 ± 2.6	14.0 ± 0.3	8.3 ± 2.2
Biochar-HTSI-7	84.0 ± 2.7	9.9 ± 0.3	6.2 ± 2.4

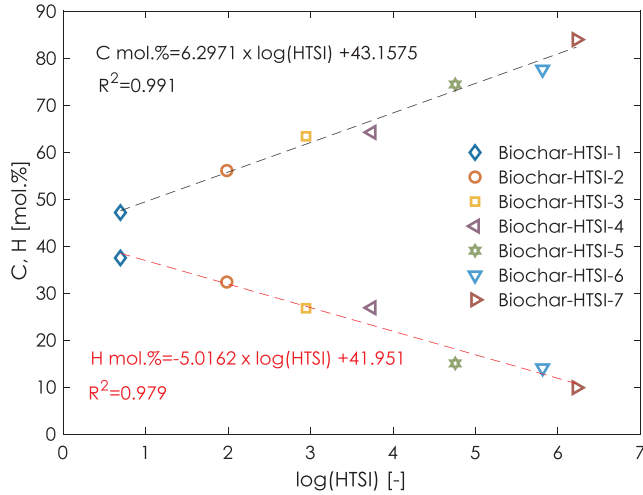


**Fig. 3.** Evolution of C and H molar contents with HTSI.

### 3.3. Chemical composition

The chemical composition of the biochar samples is given in the Table 3. The C content increases from 47.1 mol% for the biochar-HTSI-1 to 84 mol% for the biochar-HTSI-7, reflecting C enrichment of the biochar when increasing the severity. This C enrichment is accompanied by a release of H and O atoms to the gas phase and a progressive ordering of the biochar structure [42].

Fig. 3 shows the evolution of C and H molar contents as a function of the HTSI natural logarithm. We can observe that the two molar ratios are remarkably correlated to the natural logarithm of HTSI following linear relationships:

$$Cmol. \% = 6.2971 \log(HTSI) + 43.1575 \quad (3)$$

$$Hmol. \% = -5.0162 \log(HTSI) + 41.951 \quad (4)$$

The linear dependence of O content on the logarithm of HTSI is less accurate. These derived relationships imply that at very high HTSI values (~8000) which corresponds to highly severe conditions, the Cmol. % tends toward 100% while H mol. % tends towards zero approaching the chemical composition of glass-like carbon.

The closeness of the chemical composition of biochar-HTSI-3 and biochar-HTSI-4, prepared respectively at 600 °C and 800 °C (Table 3) was very surprising for us, regarding the high temperature difference of 200 °C. However, in the light of the established HTSI definition, for which the values for biochar-HTSI-3 and biochar-HTSI-4 are close, those interrogations find plausible explanations. Indeed, the fact the biochar-HTSI-3 resided more in the reactor than the biochar-HTSI-4, would have resulted in more O and H emission to the gas phase, which bring the chemical composition of biochar-HTSI-3 quite close to that of biochar-HTSI-4. Similar observations have been made in the literature by Yip et al. [9] who obtained similar carbon content for wood chars obtained at 900 °C without a hold time and wood pyrolyzed at 750 °C

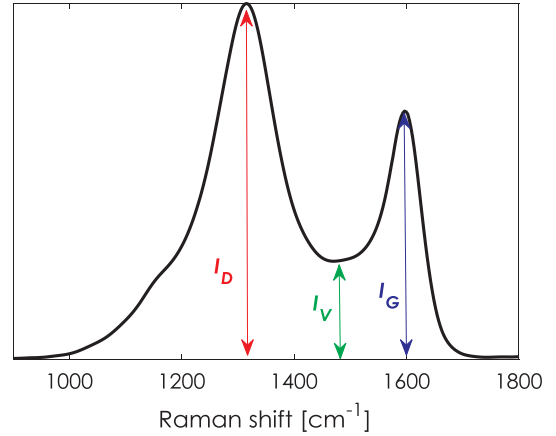


**Fig. 4.** Example of the Biochar-HTSI-7 Raman spectra and illustration of D band, G band and Valley region intensities.

with a dwell time of 600 min. Even if the results concerned slow pyrolysis (10 K/min), the O and H emission to the gas phase was effective and may be greater for a high heating rate nascent biochar like those of the present study obtained from entrained flow pyrolysis.

Controlling the chemical composition of chars is relevant to many applications such as tar removal by adsorption on biochar, which depends on its carbon content [43]. Moreover, the carbon content of the biochar can be seen as an indicator of the stability of the biochar in the soil when focusing on application of soil quality improvement or carbon sequestration for global warming mitigation [7].

### 3.4. Structural changes of the biomass particles as revealed by Raman spectroscopy

Increasing the pyrolysis temperature strongly affects the biochar structure as agreed and discussed in the literature [44–47]. In our previous work, we reported the evolution of the biochar structure in function of the reactor temperature using Raman spectroscopy [28]. The characteristic bands are illustrated in Fig. 4. Their intensity ratios,  $\frac{I_D}{I_G}$ ,  $\frac{I_V}{I_G}$  and  $\frac{I_V}{I_D}$  are representative of the biochar structure. The values of these ratios, as well as that of the total Raman area TRA are reported in Table 4.

These band intensity ratios are illustrative of the structural ordering in the biochar. For instance, the  $\frac{I_V}{I_G}$  intensity ratio was observed to decrease with the temperature following a power law [15]. Also, we reported and discussed the increase of  $\frac{I_D}{I_G}$  ratio, as well as the decrease of  $\frac{I_V}{I_G}$  and  $\frac{I_V}{I_D}$  ratios with the reactor temperatures [28]. In another study, the D band area was seen to increase with the heat treatment time for a Western Australia mallee wood biochar, especially in the early stage after the nascent biochar formation [42].

As the biochar structure depends on the temperature and heat treatment time, the Raman structural parameters should be in some ways correlated to the HTSI. This is what we found for the  $\frac{I_D}{I_G}$  and  $\frac{I_V}{I_D}$  ratios.

**Table 4**  
Total Raman Area (TRA), ID/IG, IV/ID and IV/IG ratios for the different chars.

Sample	TRA	$\frac{ID}{IG}$	$\frac{IV}{IG}$	$\frac{IV}{ID}$
Biochar-HTSI-1	410.87 ± 10.23	0.76 ± 0.05	0.82 ± 0.05	1.08 ± 0.04
Biochar-HTSI-2	418.53 ± 8.01	0.82 ± 0.03	0.74 ± 0.05	0.91 ± 0.05
Biochar-HTSI-3	368.25 ± 12.67	0.81 ± 0.07	0.65 ± 0.05	0.80 ± 0.03
Biochar-HTSI-4	438.93 ± 15.86	0.90 ± 0.08	0.62 ± 0.05	0.69 ± 0.07
Biochar-HTSI-5	411.66 ± 14.34	1.01 ± 0.05	0.62 ± 0.05	0.62 ± 0.05
Biochar-HTSI-6	362.75 ± 16.22	1.20 ± 0.06	0.63 ± 0.05	0.53 ± 0.05
Biochar-HTSI-7	254.78 ± 12.35	1.44 ± 0.04	0.39 ± 0.05	0.27 ± 0.03

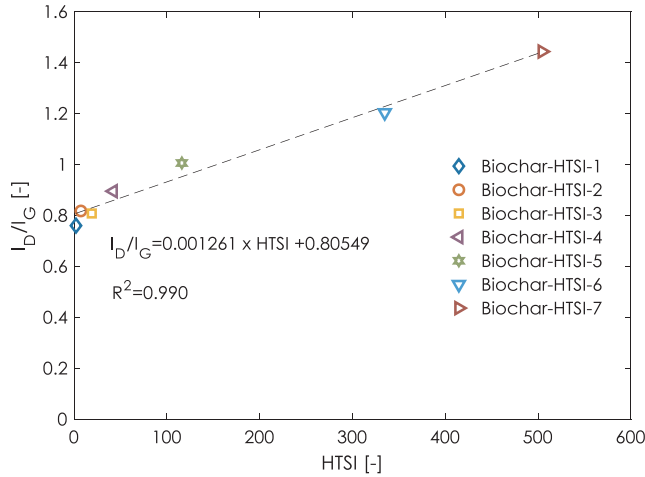


Fig. 5.  $I_D/I_G$  as a function of HTSI.

Indeed, as shown in Fig. 5, the ratio  $\frac{I_D}{I_G}$ , which represents the ratio of large aromatic ring clusters showing defects to the graphitic ones is found to be remarkably correlated with the HTSI following a linear relationship ( $R^2 > 0.99$ ):

$$\frac{I_D}{I_G} = 0.001261HTSI + 0.80549 \quad (5)$$

The  $\frac{I_D}{I_G}$  ratio is proportional to the number of ordered rings in amorphous carbons [48]. D-band signal requires ordered graphene-like domains within a few nanometers of disorder or defects to be 'activated'. The maximum  $\frac{I_D}{I_G}$  ratio typically occurs once inter-defect distances or graphene-like domain sizes are around 2–4 nm. The formation of structures which produce D band signal from the condensation of small aromatic ring clusters increases at higher HTSI [28]. This condensation of small aromatic systems into larger ones is temperature and heat treatment time dependent as found in [42].

To the authors best knowledge, there is no correlation in the literature establishing the dependence of the biomass biochar structure to those two structure-influencing parameters.

The correlation between the biochar structure and the HTSI is verified also, as shown in Fig. 6, by the linear dependence of the structural ratio  $\frac{I_V}{I_D}$  to the logarithm of HTSI ( $R^2 > 0.96$ ):

$$\frac{I_V}{I_D} = -0.12736\log(HTSI) + 1.1744 \quad (6)$$

The parameter  $\frac{I_V}{I_D}$  represents the ratio of the small aromatic systems

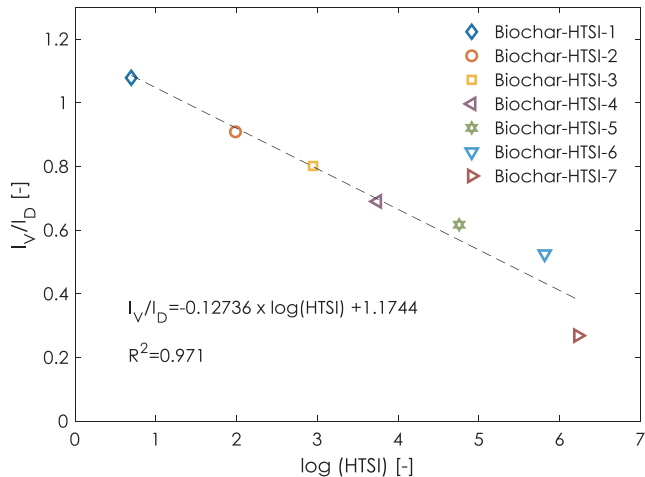


Fig. 6.  $I_V/I_D$  as a function of  $\log(HTSI)$ .

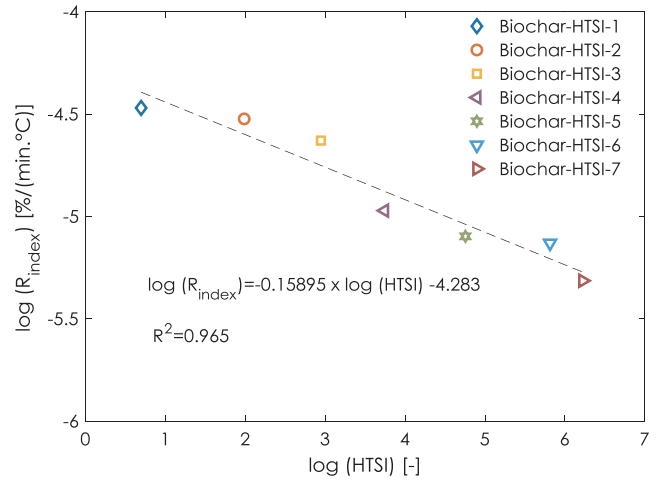


Fig. 7. Mean char reactivity index as a function of  $\log(HTSI)$ .

(< 6 rings) to the larger ones bearing defects (D band-related structures). The correlation between  $\frac{I_V}{I_D}$  and HTSI, implies a conversion of  $sp^3$ -rich amorphous carbon along with increasing growth in nanometer-sized graphene-like domains (or condensed poly-aromatic clusters with > 6 rings).

### 3.5. Reactivity towards $O_2$

The biochar reactivity indexes were determined from reactivity tests in air atmosphere using a TGA. Those values were in our previous study and the reactivity index was found to be correlated to the IV/ID ratio [28], meaning that the biochar reactivity decreases with a higher structural order of the chars. When analyzing the evolution of the reactivity index with the HTSI, we noticed that these two parameters were correlated following a power law as shown in Fig. 7. The following relationship can be derived:

$$\log(R_{index}) = -0.15895\log(HTSI) - 4.283 \quad (7)$$

This decrease in reactivity could be related to the departure of O from the biochar surface as well as to the structural ordering of the biochar matrix as revealed by the Raman spectroscopy analysis. Such observations on the decrease of the biochar reactivity with the pyrolysis temperature were also reported in other studies [45,21].

### 3.6. Fixing the $T_{Ref}$ value

The  $T_{Ref}$  value affects directly the quality of the fit for the different identified correlations. The variation of the different correlation coefficients, obtained for the different linear relationships, with  $T_{Ref}$  is illustrated in Fig. 8. One can see that  $R^2$  increases with  $T_{Ref}$  for the correlations involving the biochar yield and ID/IG. It is almost constant for the correlation related to H mol% and increases for that related to C mol% in the low temperature range before becoming almost constant.  $R^2$  decreases with  $T_{Ref}$  for the correlations involving the reactivity index and the IV/ID ratio. In the present work, we chose to fix the value of  $T_{Ref}$  at 573 K. This temperature corresponds almost to the beginning of the pyrolysis process and leads to the highest average  $R^2$  when taking into account all the identified correlations between HTSI and the analyzed biochar properties.

## 4. Conclusion

In this study, we reported a new dimensionless number called the Heat Treatment Severity Index (HTSI), as a new metric for the thermal treatment severity in the process of biomass entrained flow pyrolysis. This new HTSI takes into account both effects of reactor temperature

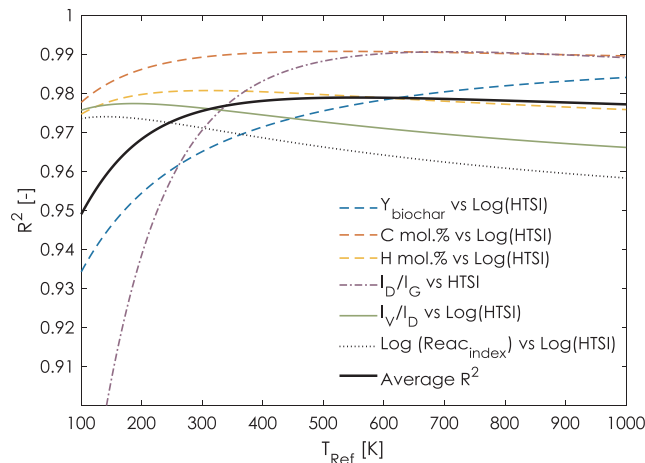


Fig. 8. Evolution of  $R^2$  for the different identified correlations as a function of  $T_{Ref}$ .

and heat treatment time, which are known to affect the biomass biochar properties. We found that the chemical, structural and reactivity properties of biochars obtained via an entrained flow pyrolysis of 370  $\mu\text{m}$  beech wood particles are correlated in remarkable ways with the HTSI. HTSI based models could potentially be used to predict biochar properties from production conditions though this will require further validation.

We think that this new idea of HTSI has to be further investigated and validated with extended experimental studies including other biochar properties, other biomasses and reactor technologies. This new parameter could constitute a new and rapid measure of the heat treatment severity in the process of biochar production in order to control their properties for defined applications.

## Acknowledgments

The authors gratefully thank the reviewers for their valuable contribution in improving this work.

## References

- McKendry P. Energy production from biomass (part 2): Conversion technologies. *Bioresour Technol* 2002;83(1):47–54.
- Basu P. Biomass gasification and pyrolysis: practical design and theory. Elsevier; 2010.
- Schmidt H-P. 55 Uses of Biochar. *Ithaka J*. 2012;25(1/2012):13–25.
- Ghouma I, Jeguirim M, Dorge S, Limousy L, Matei Ghimbeu C, Ouederni A. Activated carbon prepared by physical activation of olive stones for the removal of  $\text{NO}_2$  at ambient temperature. *Comptes Rendus Chim* 2015;18(1):63–74.
- Guizani C, Escudero Sanz FJ, Salvador S. Influence of temperature and particle size on the single and mixed atmosphere gasification of biomass char with  $\text{H}_2\text{O}$  and  $\text{CO}_2$ . *Fuel Process Technol* 2015;134:175–88.
- Kan T, Strezov V, Evans TJ. Lignocellulosic biomass pyrolysis: A review of product properties and effects of pyrolysis parameters. *Renew Sustain Energy Rev* 2016;57:126–1140.
- Crombie K, Mašek O, Sohi SP, Brownsort P, Cross A. The effect of pyrolysis conditions on biochar stability as determined by three methods. *GCB Bioenergy* 2013;5(2):122–31.
- Williams PT, Besler S. The influence of temperature and heating rate on the slow pyrolysis of biomass. *Renew Energy* 1996;7(3):233–50.
- Yip K, Xu M, Li CZ, Jiang SP, Wu H. Biochar as a fuel: 3. Mechanistic understanding on biochar thermal annealing at mild temperatures and its effect on biochar reactivity. *Energy Fuels* 2011;25(1):406–14.
- Uchimiya M, Wartelle LH, Klasson KT, Fortier CA, Lima IM. Influence of pyrolysis temperature on biochar property and function as a heavy metal sorbent in soil. *J Agric Food Chem* 2011;59(6):2501–10.
- Onay O, Kockar OM. Slow, fast and flash pyrolysis of rapeseed. *Renew Energy* 2003;28(15):2417–33.
- Kim P, et al. Surface functionality and carbon structures in lignocellulosic-derived biochars produced by fast pyrolysis. *Energy Fuels* 2011;25(10):4693–703.
- Figueiredo JL, Pereira MFR, Freitas MMA, Orfao JJM. Modification of the surface chemistry of activated carbons. *Fuel* 1999;37:1379–89.
- Bourke J, Manley-Harris M, Fushimi C, Dowaki K, Nunoura T, Antal MJJ. Do all carbonized charcoals have the same chemical structure? 2. A model of the chemical structure of carbonized charcoal. *Ind Eng Chem Res* 2007;46:5954–67.
- McDonald-Wharry J, Manley-Harris M, Pickering K. Carbonisation of biomass-derived chars and the thermal reduction of a graphene oxide sample studied using Raman spectroscopy. *Carbon N Y* 2013;59:383–405.
- Keown DM, Li X, Hayashi JI, Li CZ. Characterization of the structural features of char from the pyrolysis of cane trash using Fourier transform-Raman spectroscopy. *Energy Fuels* 2007;21(3):1816–21.
- Zhao L, Cao X, Mašek O, Zimmerman A. Heterogeneity of biochar properties as a function of feedstock sources and production temperatures. *J Hazard Mater* 2013;256–257:1–9.
- Brewer CE, Schmidt-rohr K, Satrio JA, Brown RC. Characterization of biochar from fast pyrolysis and gasification systems. *Environ Prog Sustain Energy* 2009;28(3).
- Bourauzi Z, Jeguirim M, Guizani C, Limousy L, Dupont C, Gadiou R. Thermogravimetric study on the influence of structural, textural and chemical properties of biomass chars on  $\text{CO}_2$  gasification reactivity. *Energy* 2015;88:703–10.
- McDonald-wharry J. Biochars and carbonised biomass: a new zealand perspective with a focus on chemistry. *Chem New Zeal* 2014;2014:29–33.
- Morin M, Pécate S, Hémati M, Kara Y. Pyrolysis of biomass in a batch fluidized bed reactor: effect of the pyrolysis conditions and the nature of the biomass on the physicochemical properties and the reactivity of char. *J Anal Appl Pyrol* 2016;122:511–23.
- Potgieter-Vermaak S, Maledi N, Wagner N, Van Heerden JHP, Van Grieken R, Potgieter JH. Raman spectroscopy for the analysis of coal: A review. *J Raman Spectrosc* 2011;42(2):123–9.
- Bar-Ziv E, Zaida A, Salatino P, Senneca O. Diagnostics of carbon gasification by raman microprobe spectroscopy. *Proc Combust Inst* 2000;28(2):2369–74.
- Zaida A, Bar-Ziv E, Radovic LR, Lee Y-J. Further development of Raman Microprobe spectroscopy for characterization of char reactivity. *Proc Combust Inst Jan*. 2007;31(2):1881–7.
- Sheng C. Char structure characterised by Raman spectroscopy and its correlations with combustion reactivity. *Fuel Oct*. 2007;86(15):2316–24.
- Guizani C, Valin S, Billaud J, Peyrot M, Salvador S. Biomass fast pyrolysis in a drop tube reactor for bio oil production: experiments and modeling. *J. Anal. Appl Pyrolysis* 2017.
- Billaud J, Valin S, Peyrot M, Salvador S. Influence of  $\text{H}_2\text{O}$ ,  $\text{CO}_2$  and  $\text{O}_2$  addition on biomass gasification in entrained flow reactor conditions: Experiments and modelling. *Fuel* 2016;166:166–78.
- Guizani C, Jeguirim M, Valin S, Limousy L, Salvador S. Biomass chars: the effects of pyrolysis conditions on their morphology, structure, chemical properties and reactivity. *Energies* 2017;10(6):796.
- Guizani C, Haddad K, Limousy L, Jeguirim M. New insights on the structural evolution of biomass char upon pyrolysis as revealed by the Raman spectroscopy and elemental analysis. *Carbon NY* 2017;119.
- Ruiz HA, Thomsen MH, Trajano HL. Hydrothermal processing in biorefineries: production of bioethanol and high added-value compounds of second and third generation. *Biomass* 2017.
- Jeder A, et al. The severity factor as a useful tool for producing hydrochars and derived carbon materials. *Environ Sci Pollut Res* 2018;25(2):1497–507.
- Pyle LA, Hockaday WC, Boutton T, Zygourakis K, Kinney TJ, Masiello CA. Chemical and isotopic thresholds in charring: implications for the interpretation of charcoal mass and isotopic data. *Environ Sci Technol* 2015.
- Commandré JM, Salvador S, Van Steene LDE, Gadiou R. The formation and reduction of no during the combustion of powdered petroleum coke – The case of cement plant precalciner conditions. *Combust Sci Technol* 2005;177(3):579–611.
- Septien Stringel S. High temperature gasification of millimetric wood particles between 800 °C and 1400 °C. Université de Toulouse, Institut National Polytechnique de Toulouse 2011.
- Billaud J, Valin S, Ratel G, Thiery S, Salvador S. Biomass gasification between 800 and 1, 400 °C in the presence of  $\text{O}_2$ : drop tube reactor experiments and simulation. *Chem Eng Trans* 2014;37(2013):163–8.
- Septien S, Valin S, Dupont C, Peyrot M, Salvador S. Effect of particle size and temperature on woody biomass fast pyrolysis at high temperature (1000–1400 °C). *Fuel* 2012;97:202–10.
- Chen L. Fast pyrolysis of millimetric wood particles between 800 °C and 1000 °C. Claude Bernard Lyon I 2009.
- Gorton CW, Kovac RJ, Knight JA, Nygaard TI. Modeling pyrolysis oil production in an entrained-flow reactor. *Biomass* 1990;21:1–10.
- Gheorghe C, Marculescu C, Badea A, Dinca C, Apostol T, CNCIS. Effect of pyrolysis conditions on bio-char production from biomass. 3rd WSEAS Int. Conf. Renew. Energy Sources. 2009. p. 239–41.
- Trubetskaya A, Jensen PA, Jensen AD, Steibel M, Spliethoff H, Glarborg P. Influence of fast pyrolysis conditions on yield and structural transformation of biomass chars. *Fuel Process Technol* 2015;140:205–14.
- Elyoussi K, Blin J, Halim M. High-yield charcoal production by two-step pyrolysis. *J Anal Appl Pyrol* 2010;87(1):138–43.
- Yip K, Xu M, Li C-Z, Jiang SP, Wu H. Biochar as a Fuel: 3. mechanistic understanding on biochar thermal annealing at mild temperatures and its effect on bio-char reactivity. *Energy Fuels Jan*. 2011;25(1):406–14.
- Paethanom A, Yoshikawa K. Influence of pyrolysis temperature on rice husk char characteristics and its tar adsorption capability. *Energies* 2012;5(12):4941–51.
- Smith MW, et al. Structural analysis of char by Raman spectroscopy: Improving band assignments through computational calculations from first principles. *Carbon NY* 2016;100:678–92.
- Asadullah M, Zhang S, Min Z, Yimsiri P, Li C-Z. Effects of biomass char structure on its gasification reactivity. *Bioresour Technol* 2010;101(20):7935–43.



- [46] Azargohar R, Nanda S, Kozinski JA, Dalai AK, Sutarto R. Effects of temperature on the physicochemical characteristics of fast pyrolysis bio-chars derived from Canadian waste biomass. *Fuel* 2014;125:90–100.
- [47] Li X, Hayashi J, Li C. FT-Raman spectroscopic study of the evolution of char structure during the pyrolysis of a Victorian brown coal. *Fuel Sep.* 2006;85(12–13):1700–7.
- [48] Ferrari AC. Raman spectroscopy of graphene and graphite: Disorder, electron-phonon coupling, doping and nonadiabatic effects. *Solid State Commun* 2007;143(1–2):47–57.